Water Resources Research

RESEARCH ARTICLE

10.1029/2021WR031567

Key Points:

- The height of an obstacle is the controlling factor on any sound-stage relationship
- Monitoring sound above the height of an obstacle is possible due to continued free-surface effects
- The production of sub-aerial sound is primarily produced by white water

Correspondence to:

W. A. Osborne,
william.a.osborne@durham.ac.uk

Citation:

Osborne, W. A., Hodge, R. A., Love, G. D., Hawkin, P., & Hawkin, R. E. (2022). The influence of in-channel obstacles on river sound. *Water Resources Research*, *58*, e2021WR031567. https://doi.org/10.1029/2021WR031567

Received 5 NOV 2021
Accepted 21 MAR 2022

The Influence of In-Channel Obstacles on River Sound

William A. Osborne[1], Rebecca A. Hodge[1], Gordon D. Love[2], Peter Hawkin[3], and Ruth E. Hawkin[3]

[1]Department of Geography, Durham University, Durham, UK, [2]Departments of Computer Science and Physics, Durham University, Durham, UK, [3]Evolto, Haltwhistle, UK

Abstract The sound of a river can change from a babbling brook to a thunderous torrent, and we have previously shown that there is the potential to predict river stage from the river's sub-aerial sound. Here, we examined how alterations in channel configuration can change the relationship between stage and sound pressure level using a white water course to simulate a real-world scale channel. By using blocks as roughness elements (REs), we were able to customize the course's obstacles, creating towers of different heights and placements. We then ran a varied flow discharge of up to 10 $m^3 s^{-1}$. We used data collected from microphones, a hydrophone and cameras to monitor the flow and to understand the processes occurring. In addition to sound processing, we used image analysis to calculate the area of white water on the surface of the water to determine the mechanism for sound production. Our analysis showed the likeliest source of sub-aerial sound is from white water being produced from the flow's interaction with the REs, with the relationship between white water value and sound relationship having an R^2 between 0.35 and 0.82. In terms of influence on sound, we found that the height of the REs is more important than their spatial distribution, with the taller the RE, the better the logarithmic relationship between sound and stage. We suggest that monitoring in a natural setting will work best in the places with the tallest obstacles and that the quality of the sound-stage relationship is dependent on RE height.

1. Introduction

Rivers can be variable, noisy environments, able to change from a babbling brook to a thunderous torrent. There is evidence to suggest that the flow controls the range of sounds produced by a river, including seismic (ground vibrations), hydroacoustic (underwater), infrasonic (sub-aerially at < 20 Hz), and human-audible acoustics (sub-aerially at 20 Hz to 20 kHz; Manasseh et al., 2006; Morse et al., 2007; Osborne et al., 2021; Ronan et al., 2017; Schmandt et al., 2017). Human-audible sound produced sub-aerially has been shown to correlate with a river's stage, providing a non-intrusive way to monitor a river (Osborne et al., 2021). Using sub-aerial sound to monitor a river's stage is potentially a non-intrusive method of measuring, such as for flood monitoring, when other methods such as pressure transducers or ultrasonic depth monitors aren't safe to deploy. This method could be especially useful in the seldom monitored headwater catchments, which make up 70%–80% of total catchment area, whose morphology is characterized by rough beds (Gomi et al., 2002). The sound of the river is determined by the interaction of the flow with the bed topography. Our previous work has demonstrated the role of roughness elements (REs) in producing noise, but we do not know how factors such as RE size and spacing affect noise production. To determine the effect of the bed topography on the flow, and the sound it produces, we designed an experiment using a white water course (WWC), allowing the channel bed to be altered through the addition of REs. Our findings will aid future work using sound to monitor stage as it will identify sections of a river that will provide the best chances of finding a sound-stage relationship. We turn to two areas of hydraulics that introduce aspects of how the bed topography of a river can influence its flow; flow resistance and white water generation.

Flow resistance is formed by features within a channel that oppose the flow, generating turbulence, and depends on channel topography and bed texture and discharge (Venditti, 2013). Understanding flow resistance is critical for applications including flood prediction/management and channel design, such as in civil engineering (Ferguson, 2010; Powell, 2014). The flow resistance of a river channel is likely to be linked to the production of sub-aerial sound. We collected audio data from a range of different rivers, and we found that REs have an effect on the sound produced sub-aerially and suggested that they are the probable cause for sound production in a river (Osborne et al., 2021). To compare different rivers, relative submergence is used as a way to determine the scale of an object relative to the flow depth (Weichert et al., 2006). Herbich and Shulits (1964) suggested that resistance at flow depths greater than RE height is related to the pattern and spacing of the REs. Bathurst (1978) noted that unless all the taller REs protrude from the flow, then there will be spatial differences in the flow regime, with the wake from one RE affecting the flow around downstream REs. Water will be forced around an obstacle (producing buffer waves) when relative submergence is low, but as stage increases, the water's path will begin to change and will eventually overtop the RE (producing recirculating waves) (Kean & Smith, 2006). Therefore sound may be dependent on how closely REs are spaced and if they protrude from the flow. We take account in our experiment that the size, distribution and state of protrusion of the obstacles can have an effect on the flow resistance.

Sub-aerial sound is primarily generated from the surface of the water, and is formed from turbulent structures such as standing waves and eddy currents forming white water (Bolghasi et al., 2017). Air becomes trapped within the water, known as self-aeration, when there are flow discontinuities generating white water locally, which is both air trapped within the water, and air coated in water (Chanson, 2012; Rodi, 2010). In flume studies of supercritical flow, where flow was forced to diverge or overtop a structure, air cavities built and led to "loud noises" being formed (Chanson & Toombes, 1998). In terms of energy, we can think of this as a turbulent energy cascade, in which the initial large scale eddies break down into progressively smaller and smaller eddies until they are small enough that friction removes the remaining energy (Kolmogorov, 1949). In doing so, the bubbles generated from turbulent eddies break up further into smaller, and smaller bubbles (bubble-mass cascade) (Chan et al., 2021). Bubble size and eddy size are intrinsically linked, with large eddies advecting bubbles and small eddies being unable to break them up (Chanson, 2012). Advected bubbles are then released when the shear becomes low enough. Bubbles and sound are linked with the Minnaert resonance, with the larger a bubble, the lower its corresponding frequency, such that a 10 cm bubble radius has a frequency of 32 Hz and a 1 cm radius bubble has a frequency of 326 Hz (Leighton, 1994; Minnaert, 1933). These white waters are drivers of air-water gas exchange, especially in mountain streams, where turbulence and bed roughness means that the gas exchange rate can be 96 times greater than for low-sloped, gentler rivers (Hall et al., 2012; Ulseth et al., 2019). Underwater sound production can be generated from the collision of bedload as sediment is transported downstream (Marineau et al., 2015). However, since there is no mobile bedload in our experiment, then that is not generated. While we can determine the source of the sound, there is no current way of linking the white water to the sub-aerial sound that is being produced and how it is related to RE size or configuration. Our experiment will examine how the area of white water found on the surface relates to the sub-aerial sound.

Our focus here is on the sub-aerial sound produced by a river and how that is connected with REs. However, in our experiments, we also record underwater sound as a basis of comparing if what is observed on the surface is the same as underwater sound. Our study aims to investigate if: (a) there is a link between the sound produced and the height of a RE; (b) layout of REs has any control on sound production and (c) there is a relationship between the white water area and sound pressure level (SPL).

2. Methods

2.1. Experimental Setup

The Tees Barrage International White Water Centre, Stockton-on-Tees was chosen to simulate a real scale river. Figure 1 shows photographs of the course when used for sport. The course has substantial advantages over a conventional indoor flume such as removing the need for recirculation pumps that produce noise that would obscure the audio signal. It is at a scale that is comparable to a river, but retains the same control over flow that you get in a flume (Barton et al., 2005). Being at real-life scale means our data are comparable to real-world river systems. The experiment was run over 2 consecutive days, December 9–10, 2020, on which there were cloudy but settled weather conditions.

The section of the course that we collected data in is 7.5 m wide, with a slope of 0.005, and is lined with concrete. Within the channel, obstacles can be created from RapidBlocs™ which are interlocking, stackable blocks that are able to be attached firmly to the channel bed in different configurations and can quickly be rearranged into new designs. Blocks are $1.0 \times 0.50 \times 0.25$ m and are capped with a rounded lid of $1.0 \times 0.50 \times 0.08$ m. We used these blocks to alter the channel bed, simulating different REs. Water was run through the course with a discharge up to 10 $m^3 s^{-1}$. Within the channel, the water was released using a digitally controlled and monitored bear trap gate, allowing fine control of 0.1 $m^3 s^{-1}$ in discharge and was able to sustain the desired discharge due to the large body of water being held upstream.

10.1029/2021WR031567

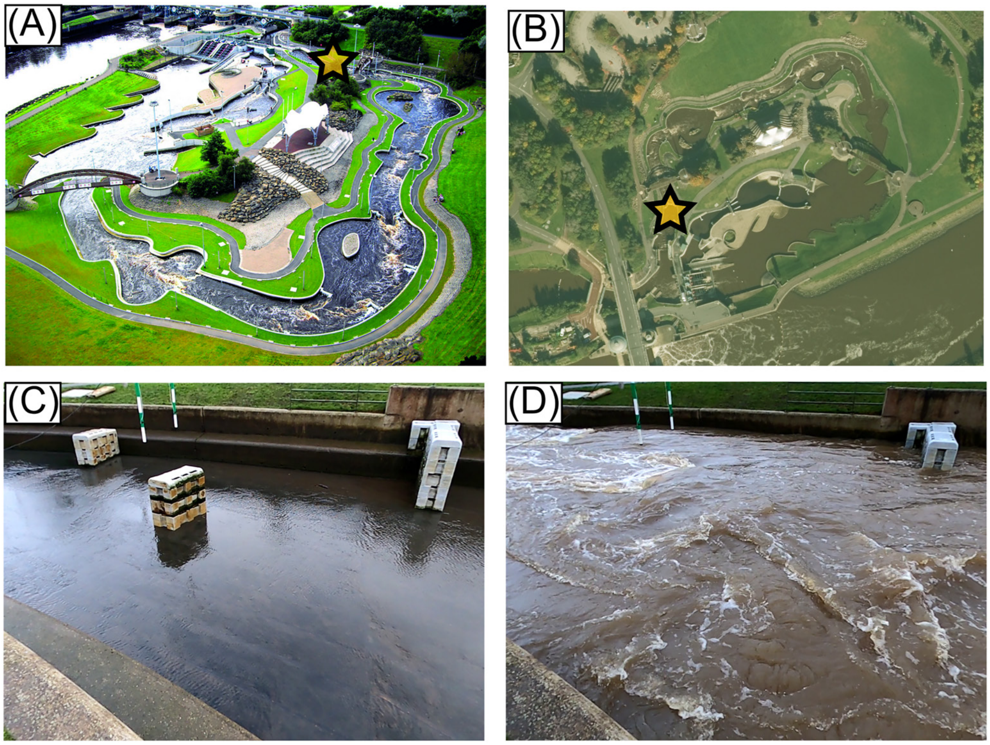

Figure 1. (a) Aerial image of the course during full flow with the star representing the area chosen for the study, (b) aerial image of course during no flow, (c) section of course used during no flow and (d) section of course during high flow. Image (a) is produced with permission of the Tees Barrage International White Water Centre and (b) OS data Crown copyright.

Our experiment involved changing the blocks within the channel and then quickly increasing the flow from zero to full discharge, before gradually ramping down the discharge. The course was initially configured for white water sports, with blocks arranged to create alternating runs and hydraulic jumps. We reconfigured the upstream part of the course to remove the obstacles that created the hydraulic jumps, and to minimize the backwater effect of downstream obstacles (Figures 1c and 1d), creating a clear run that was maintained for 50 m. To increase the flow depth in our experimental section, we created a pinch point upstream and downstream of the test site, which constrained the channel. The addition of these side blocks allowed a stage above 1 m to be achieved (Figure 2a). Although these blocks are an additional RE in our measurement section, their influence will be consistent through all runs.

To monitor the WWC, four microphones were set up in an array around and above the channel (Figure 2b). In addition to sub-aerial recording, a hydrophone was placed within the channel to record underwater sound and two pressure transducers (TD-Diver) were attached to the floor in the center (D1) and the bank (D2) to monitor stage. One microphone was suspended above the center point (M4) of the test site from guide wires, with the other three located downstream (M1), centrally (M2), and upstream (M3). All the microphones were directed to the center of the test site. The microphones were covered with a windshield primarily to prevent water splashes from hitting them, but also to reduce any wind noise. Wind was however limited during the experiment at less than 5 mph. We used RØDE NTG2, which is a mid-high level supercardioid microphone, with a rejection of 150° to the rear, with a sensitivity of -36 dB re 1v/Pascal at 1 kHz. The hydrophone used was an Aquarian H2a, an omnidirectional hydrophone with a sensitivity of -170 dB re 1v/Pascal at 1 kHz. Due to the different reference values between water and air, the SPL values between them cannot be directly compared. The hydrophone was shielded from the direct flow of the course by situating it behind a set of blocks upstream of the measurement site. All microphones and the hydrophone were connected to a Zoom F6 field recorder and so could be operated at the same time. For the first two experimental runs, the hydrophone was disconnected, therefore, no data is presented for these runs. The Zoom F6 recorded each microphone simultaneously at 32-bits at 44.1 kHz in the WAV format. Our sound data is presented in sound pressure level (dB SPL). During each run, a time-lapse video was recorded from the bank of the channel near M2 using a GoPro MAX 360 at a frame rate of 1 per second.

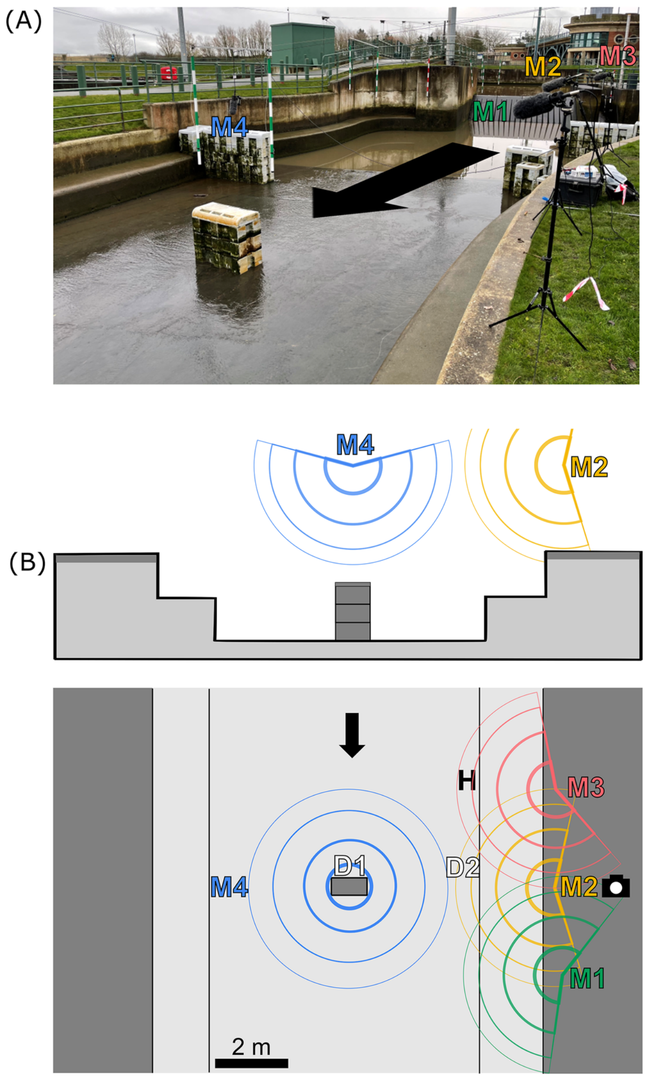

Figure 2. (a) Photograph of the white water course during experimental run LF_3 showing the proximity to the bear trap gate. (b) Schematic of the experimental setup and locations of equipment. Microphones: Downstream (M1), central (M2), upstream (M3) and over-channel (M4). Hydrophone (h), camera, and central diver (D1) and bank diver (D2). The pickup angle of the microphones is shown with the concentric circles.

2.2. Experimental Run

An experimental run typically took 15–20 min including both the increase and decrease in flow, and the rearrangement of the blocks. The blocks were set up in the following ways (Figure 3) and hereunto configurations will be referred to by the letter of the configuration, and the number of blocks, that is, $LF_{2.2}$ would be blocks with their long face perpendicular to the flow in a side by side arrangement with each side being two blocks tall and LF_n refers to all scenarios with a single tower of heights between one and four blocks. We used configurations of between one and four towers of blocks, and each tower was between one and four blocks tall. The run types are broken into two groups, simple and mixed. In simple runs, all towers had the same height, whereas in mixed runs, different towers had different heights. A run started with a dry course, and consisted of a rapid flow release of 10 $m^3 s^{-1}$, followed by a period of time to allow the flow to steady, which averaged from around 30–60 s. The discharge was then dropped in 2 $m^3 s^{-1}$ decrements, with again time being given to allow the gate to move and for the discharge to drop, averaging 1 min. As the experimental section was within 30 m of the top of the course, the flow quickly adapted to any change in discharge. We stopped the run once the flow reached 2 $m^3 s^{-1}$, as after this point, the noise of the gate draining obscured the sound produced by the REs as well as allowed foam to be produced.

2.3. Sound Processing

Producing a sound-stage relationship requires a single value for sound, which is found by processing audio through a fast Fourier transform (FFT), giving SPL for each frequency. By splitting our continuous recording into 1 s clips, it allowed a frequency resolution of 1 Hz from the FFT, meaning an SPL for each hertz from 20 Hz up to 22.05 kHz due to the microphone frequency response. A single SPL value is found by binning into kHz ranges, that is, 1–2 kHz, and then the median (spectral center) of the 1,000 SPL values within this range is taken (Osborne et al., 2021). The spectral center of the data is used as it yields a more representative signal that is not skewed by erroneously large or low values in the frequency range. Each kHz bin therefore had a single value, with the sound-stage relationship being dependent on the frequency bin chosen. Since there was no wind present during the experiments, we do not need to preprocess the data to remove any extraneous ambient noises. In Osborne et al. (2021), we showed that the sound-stage relationship was strongest at low frequencies (<3 kHz) and that not having wind noise significantly improves the data quality. We use our experimental data to test how sound-stage relationships are affected by microphone location, and whether the location affects the frequency that produces the strongest sound-stage relationship. As we are concerned with finding the best relationship possible, we needed to analyze all microphone recordings to choose the microphone that provided the best signal.

2.4. Image Processing

We used image processing to measure how the amount of white water that was produced varied through each experimental run. Video was recorded from the same location as M2 on the bank of the course, which gave an oblique view to the channel. An above water view would have been preferred, but would have been difficult to record continuously and to set up. A drone was not appropriate because its rotor noise would then have affected our sound recordings. Beneficially, the experimental days were cloudy, giving equal lighting and no shadows or

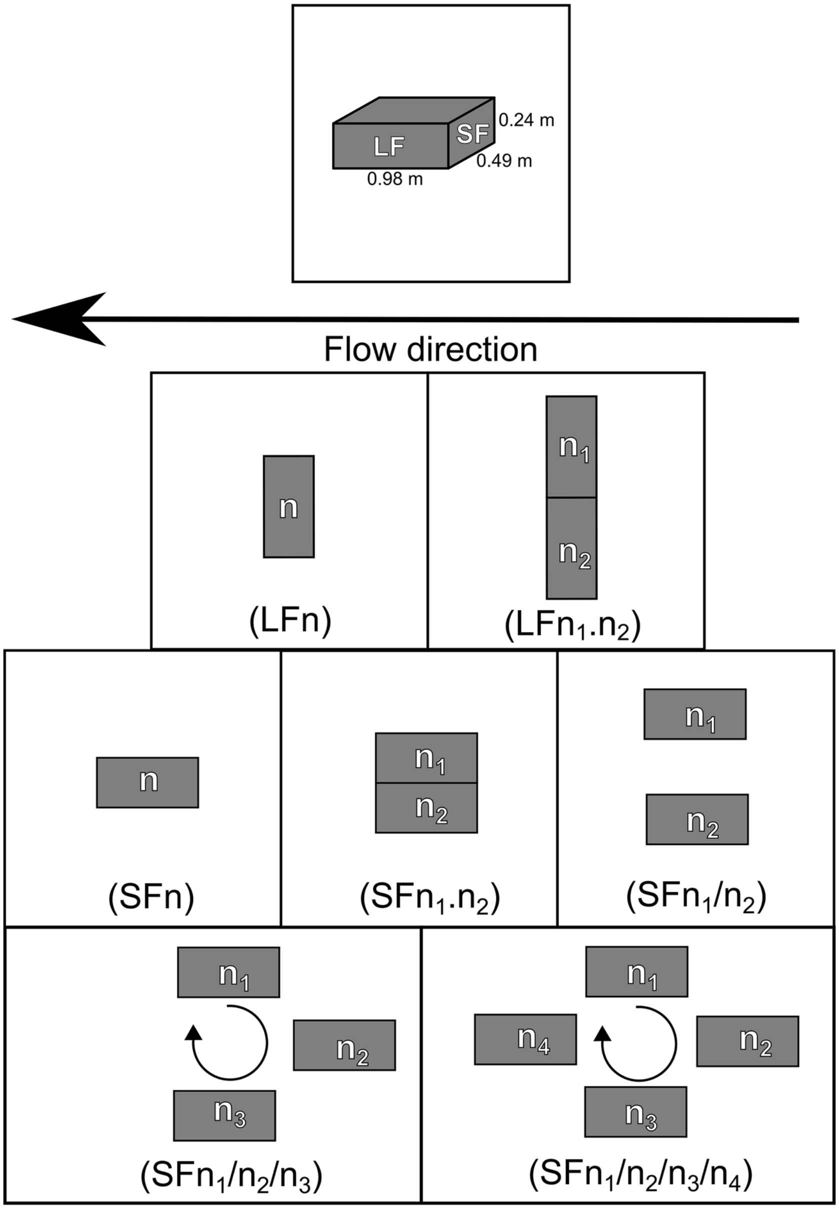

Figure 3. Block configurations when placed in the channel. LF—longest face, SF—shortest face, n—number of blocks in the tower.

glare from the water. For each experimental run, we had one video frame per second, which matched the sound processing clip length of a second. Within a frame, there were areas outwith the target area, such as the sky, that were first masked from the frame, leaving only the channel. Due to the top surface of the block being white, these were masked as well, whereas the other surfaces are dark enough to not be considered white (Figure 4). The frame was then converted into greyscale and then binarized into black (0) and white (1) using *imbinarize* in MATLAB 2021. A pixel was either assigned black or white given the threshold luminance value. Pilot tests showed that a luminescence value of 0.6 produced the best results as it kept the white water, but removed any light reflections. Noise was reduced in the binarized image, with white pixels being required to be connected to another white pixel. A connection value of 20, meaning a minimum block size of 20 white pixels, was found to be capable of removing pixels not related to white water but to also still capturing small white water areas. The equation to calculate the amount of white water in an image is

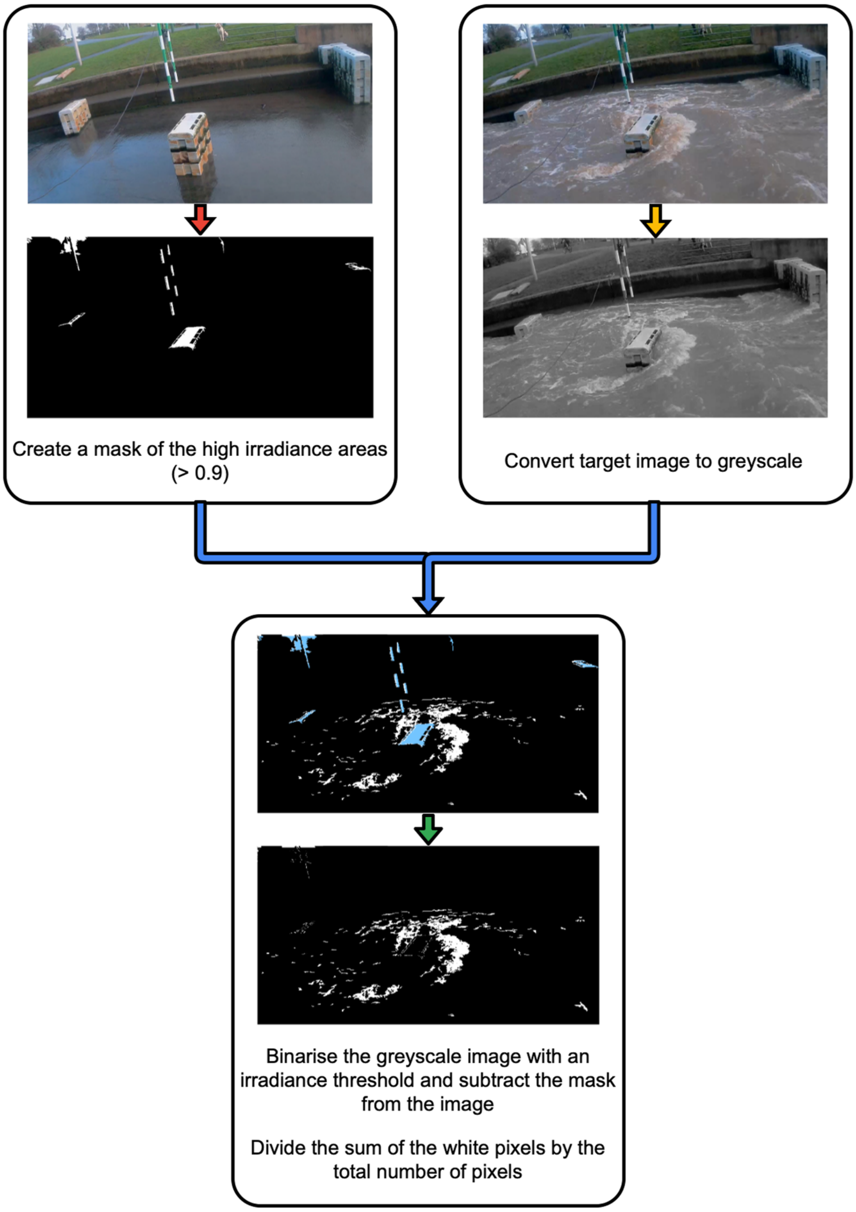

Figure 4. Flow chart of how the white water value is obtained from an image. Light blue shading indicates the masked area.

$$WWV = \log_{10}\frac{W}{T} \quad (1)$$

where W = number of white pixels and T = total number of pixels, and WWV is the white water value. A log was taken for the WWV as it is to be compared against SPL, which is also in log form. Each frame had a WWV and collectively over an entire run a change in WWV can be observed.

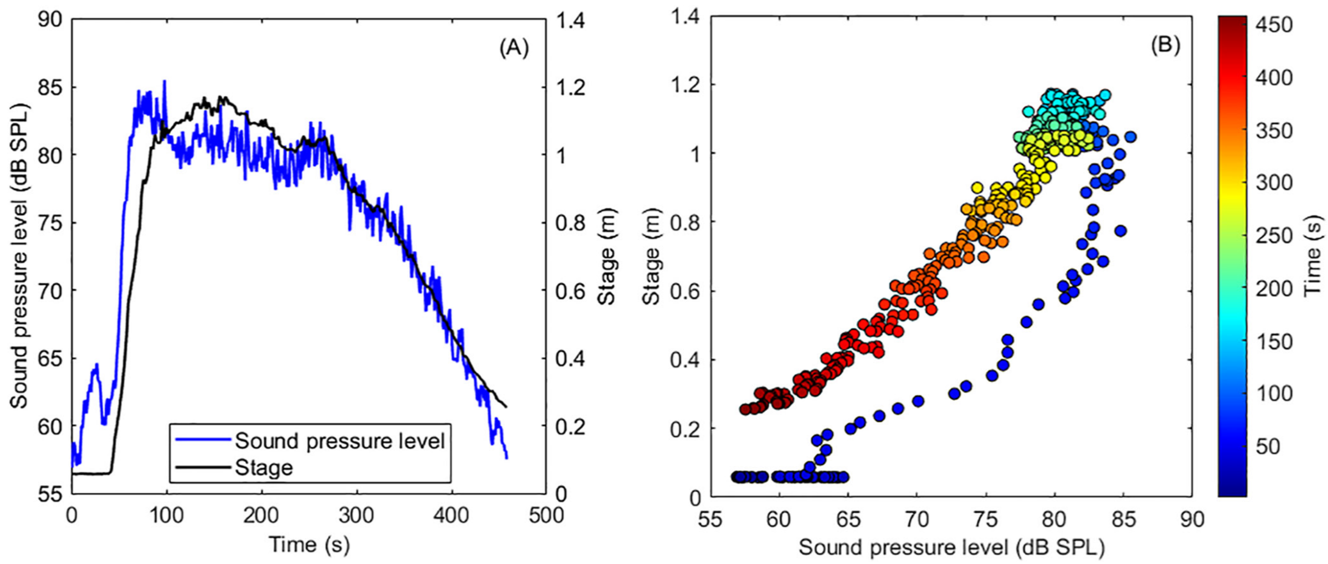

Figure 5. (a) Sonohydrograph (blue) with the stage (black) recorded from pressure transducer D2 at the bank of the channel. (b) Scatter between sub-aerial sound pressure level value and concurrent stage value.

3. Results

The results are presented in the following order: (a) analyzing the experimental runs to identify what microphones and frequency ranges are the best to use, (b) investigating the effect of RE size and configuration on sub-aerial and underwater sound, and (c) comparing how both sub-aerial and underwater sound relate to our image analysis of white water.

3.1. Microphone and Frequency Selection for Sub-aerial Sound

We present an example experimental run in Figure 5 to show the relationships between sound and stage for both the rising and falling limbs. Figure 5a shows SPL from M4 between 0.02 and 1 kHz, and stage data recorded by transducer from D2. Stage data from D1 is not used since it was highly variable due to being placed in front of an obstacle. The figure shows that stage and SPL rise and fall concurrently, with the exception of increases in sound in the first 30 s which are noises from the bear trap gate opening and not from increases in stage. We therefore disregard increases in sound before stage in all data. Figure 5b shows that there is hysteresis within the run, with the falling limb being quieter than the rising limb. The Froude number of the rising limb was 0.41 and the falling limb was 0.61 meaning subcritical flow occurred during the duration of the run. We focus our analysis on the data from the falling limb as it is more representative of a river, compared to the sudden increase of discharge with the rising limb. The longer time duration of the falling limb also means that this limb provides more data points.

To identify which microphone and frequency range to use in the subsequent analysis, for all runs and for every microphone, we plotted the stage and SPL data (as in Figure 5b) and fitted a logarithmic function to it, and generated its R^2 value. For each of the 37 runs, we identified the microphone which produced the highest R^2 using a frequency range of 0.02–1 kHz (Figure 6a). Based upon the full data set of R^2 values, there is very little difference between the R^2 values from the different microphones. To determine what frequency range to monitor, we perform the same process as for choosing the microphone. The frequency range with the highest R^2 is counted for each run, for each microphone. Figures 6b and 6c show the results from microphones M3 and M4, and it is clearly seen that lower frequencies, <2 kHz, have the highest R^2 values. M4 has 25 out of the 37 highest R^2 values in the 0.02–1 kHz bin. We therefore chose the 0.02–1 kHz bin for use in the subsequent data processing. Generally, the R^2 values drop as frequency range is increased, an observation made by Osborne et al. (2021).

With a frequency range chosen, we can analyze how the configuration of the blocks affects the R^2 values for M3 and M4 (Figures 6d and 6e). Both microphones have high R^2 values, with M3 ranging from 0.63 to 0.92 and M4

10.1029/2021WR031567

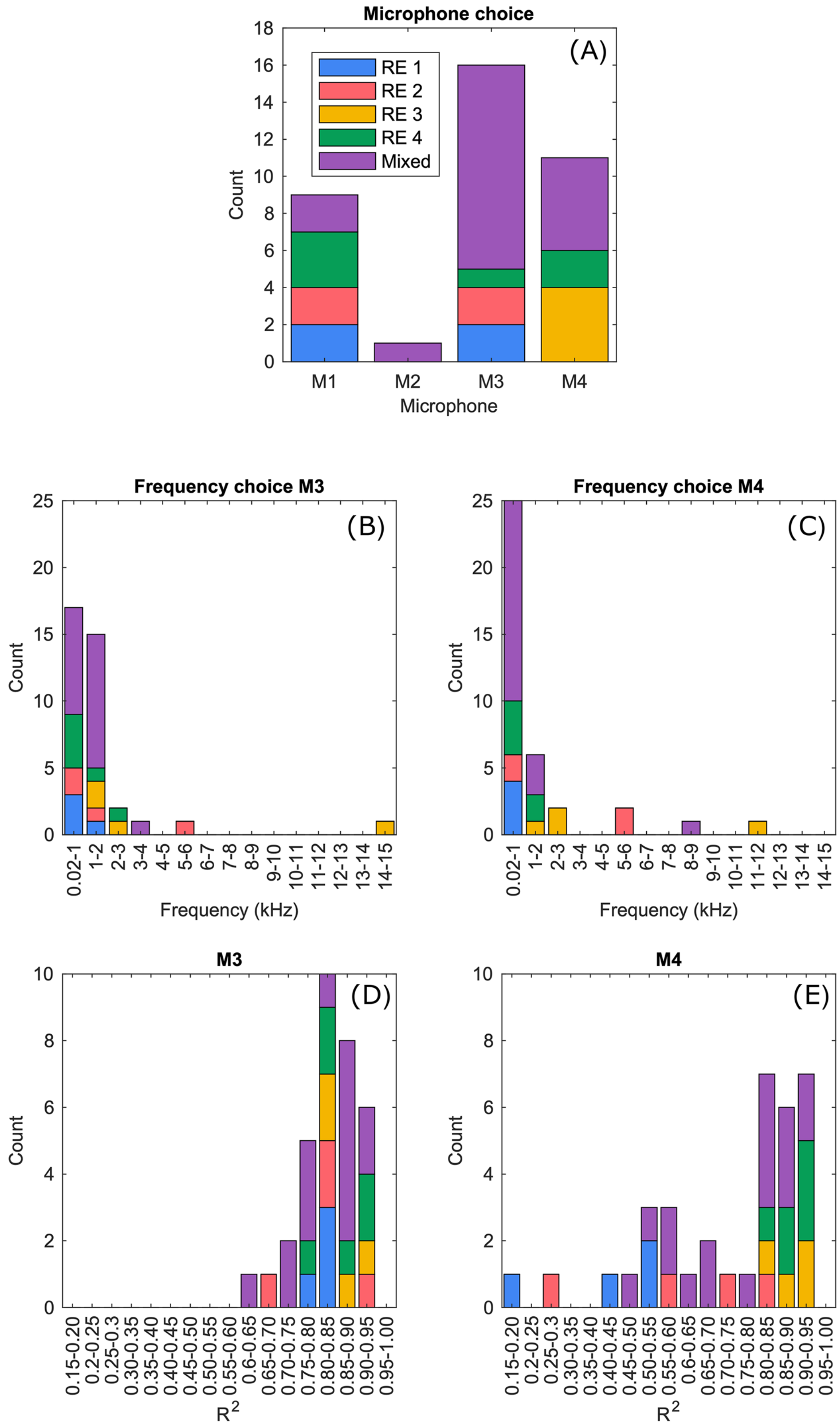

Figure 6. (a) Histogram displaying which microphone has the runs with the highest R^2 values using the frequency range 0.02–1 kHz and categorized by the roughness element height used. (b, c) Microphones 3 and 4 and the frequency range where the highest R^2 occurs. (d, e) Microphones 3 and 4 and the R^2 obtained when using the frequency range of 0.02–1 kHz.

from 0.17 to 0.94. M3 shows similar R^2 values across all block configurations, whereas with M4 R^2 values are lower for shorter REs than for higher ones. M4 is chosen in the study due to its position centrally over the channel meaning that it stays a more consistent distance from the obstacles, regardless of their configuration. We also selected M4 as we think that M3 is more affected by the noise of upstream obstacles.

3.2. The Impact of RE Height on Sub-aerial Sound

We break the runs into two groups, simple and mixed, and by the height of the REs, to clarify the results. The runs with a simple configuration show a clear relationship between sound and stage, which overall forms a logarithmic function (Figure 7). Within the overall logarithmic shape, some scenarios show kinks in the data at certain elevations. For configurations with a RE height of 1, the data is more scattered, with kinks in the data above the RE 1's height. Similarly, we see a kink in the data from runs with REs of two blocks high; however, it occurs above the height of RE 2. The kink in data is not seen in data from runs with REs of 3 and 4. The scatter of the data reduces as RE height is increased and in turn the R^2 of the logarithmic fit increases. For example, with the simplest block configuration LF_n, (where $_n$ = 1–4), R^2 increases from 0.52 to 0.91. Another factor to consider is the range of the data, and how loud the flow becomes. With an RE height of 1, SPL approximately varies between 60-dB SPL, whereas with a RE height of 4, SPL varies between 60 dB SPL.

3.3. The Impact of RE Configuration on Sub-aerial Sound

Having established that the RE height is important in the sound-stage relationship, we now see how this relationship is affected by RE configuration. Figure 8 shows all the other runs undertaken, comprising REs of varied heights, and different configurations. As with the previous configurations, as RE height is increased, the R^2 value also increases. However, the changes in R^2 as the height of the tallest RE varies from RE 1 to RE 4 is not as substantial as from the simpler configurations. The kinks observed above the submergence of an RE are still visible in the data, most notably when there are RE 1 heights. The spatial configuration has a negligible effect on the trends we are seeing, with the configuration with most blocks $SF_{4/4/4}$ having the same loudness as $SF_{4/4}$. There are differences between runs where the blocks were connected or separated, for example, $SF_{4.4}$ and $SF_{4/4}$, with the latter being marginally louder. The only configuration with the same RE height, and only a change in location, SF_4 and $SF_{0/4/0}$, has a reduced R^2 from 0.91 to 0.78. The reduction in R^2 can be attributed to the microphone being further away in $SF_{0/4/0}$. The configuration with all RE heights in the channel, $SF_{4/3/1/2}$, has an R^2 of 0.65, but it can be seen that the data kinks around the same points as when RE 1 and RE 2 are submerged. Of interest is the run in which there were no REs within the experimental section. Sound was still generated by other obstacles downstream, which in turn generated a high R^2 of 0.83, with an SPL range of 60-dB SPL. Although we have a high R^2 value, the loudness is less than in runs with obstacles in the section. Whenever an RE is within the vicinity of the microphone, it will have the effect of becoming the main signal source due to proximity, and therefore will be what we are mainly listening to during our experimental runs.

3.4. The Impact of REs on Underwater Sound

We also evaluate how the underwater sound recorded by the hydrophone varies with RE number and spacing (Figure 9). The relationship between sound and stage is not as clear as that shown with sub-aerial sound. In each run, there is a hook in the data as stage decreases from 0.6 to 0.4 m, in which sound becomes louder as stage falls. We do not have an increase in sound as stage decreases in the sub-aerial data unless there is a RE of a similar height present, but this pattern is visible in the hydrophone data at all RE height configurations. As RE height increases, there is not an increase in R^2 (unlike in Figure 7), but we have a decrease in R^2 in $LF_{4.4}$ and SF_4. There is significant scatter in the data, especially at high stages, for example, a range of dB SPL at a stage height of 0.6 m in $SF_{1.1}$.

Figure 10 shows hydrophone data for the mixed RE configurations and, as with the change from sub-aerial to underwater, there are substantial changes. There is significant scatter of the data, with R^2 values between 0.01 and 0.68. The highest R^2 of 0.68 is found with configuration $SF_{4.3}$, with all experimental runs in the $SF_{n1 \cdot n2}$ configuration having high R^2 values between 0.59 and 0.68. With no RE in the channel, there is a positive relationship between SPL and stage up until a stage of 0.6 m. Above this, SPL is constant regardless of stage.

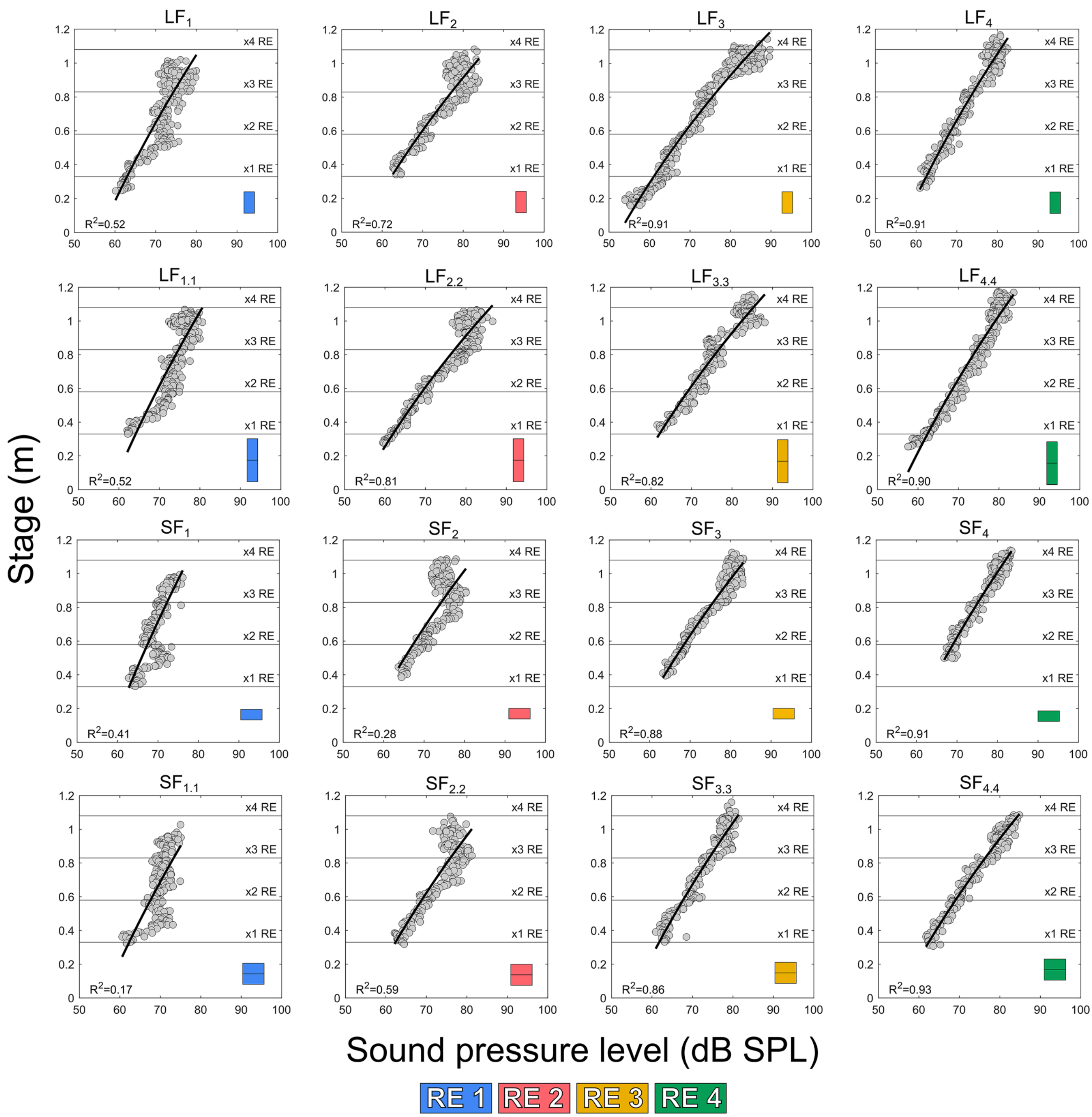

Figure 7. Plots showing the sub-aerial sound pressure level and stage recorded during the simple configuration experimental runs. Inset schematics have the block configuration color coded by the towers' height. Black line is the logarithmic function fitted to the data and the associated R^2. Horizontal lines indicate the heights of the roughness elements.

3.5. White Water Value

The white water value was calculated from only runs using configurations LF_{n1} and $LF_{n1.n2}$ (where $_{n1}$ and $_{n2} = 1$–4) due to the fall of darkness during other runs on the first day. During day 2, natural foam was generated from the Archimedes screw which severely impeded measurement of the white water produced by the REs. Figure 11 shows both the stage and WWV relationships for $LF_{4.4}$. WWV is a negative number due to being a log of a value less than one, so therefore the closer to 0 the WWV is, the more white water there is in the image. Figures 11a–11c show that the shape of a hydrograph, sonohydrograph (sound graph) and the aphrosograph (foam graph) is very

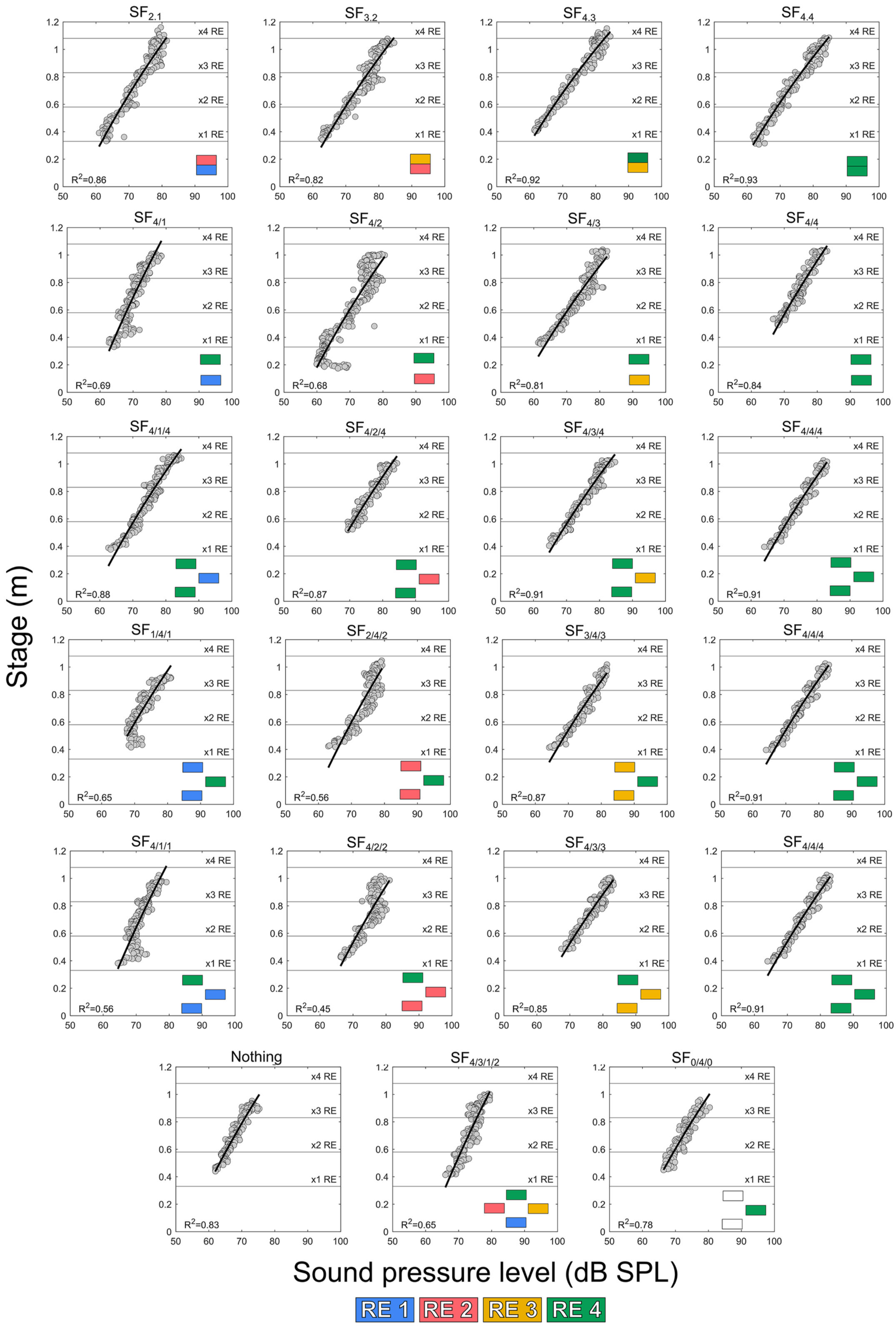

Figure 8. Plots showing the sub-aerial sound pressure level and stage recorded during the mixed configuration experimental runs. Inset schematics have the block configuration color coded by the towers' height. Black line is the logarithmic function fitted to the data and the associated R^2. Horizontal lines indicate the heights of the roughness elements.

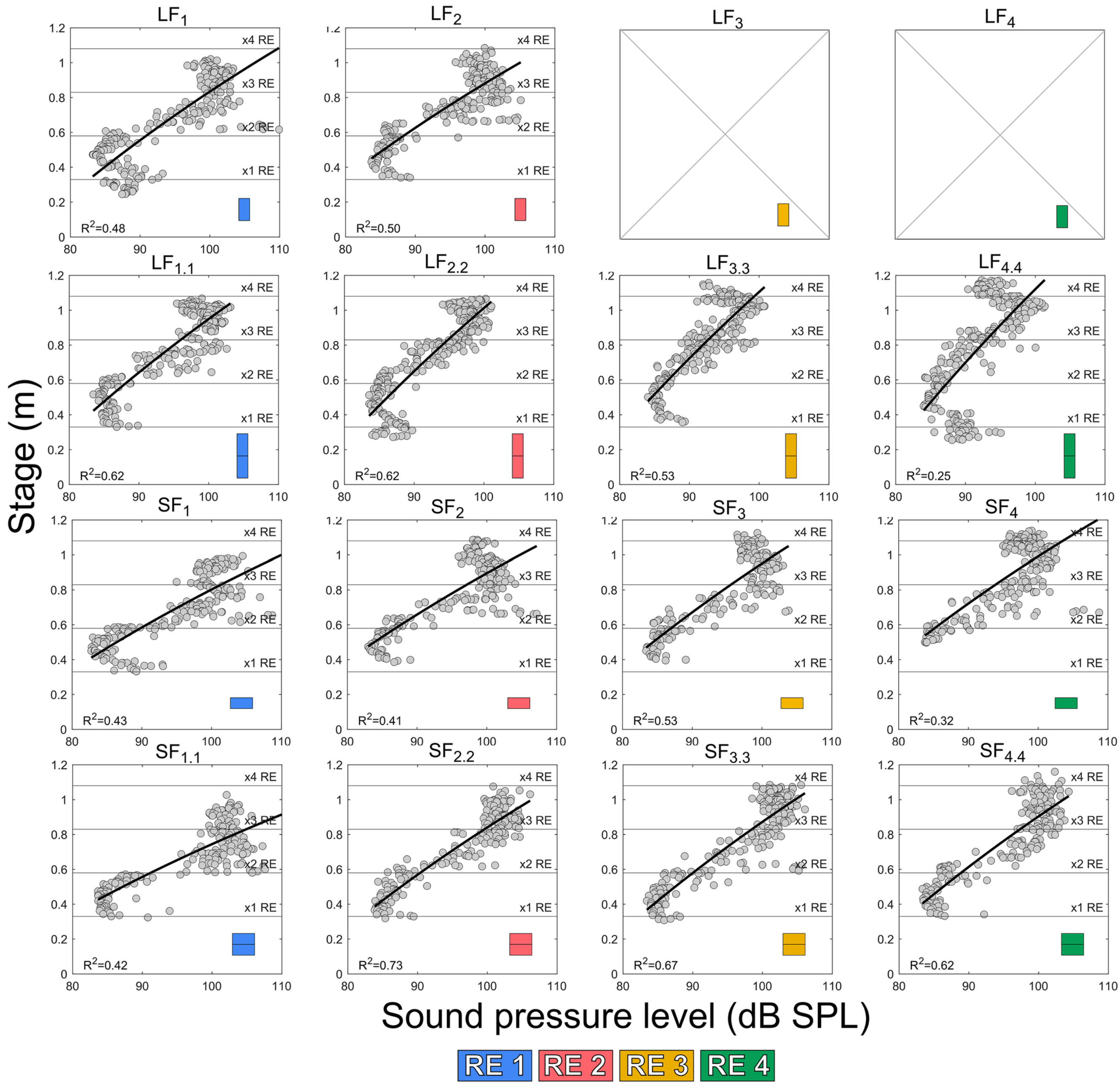

Figure 9. Plots showing the underwater sound pressure level and stage recorded during the simple configuration experimental runs. Inset schematics have the block configuration color coded by the towers' height. Black line is the logarithmic function fitted to the data and the associated R^2 printed. Horizontal lines indicate the heights of the roughness element levels. No data indicate that the hydrophone was not on during these runs.

similar. When plotted against SPL, WWV has an R^2 value of 0.73, compared to an R^2 value of 0.25 for the relationship between sound and stage for the same run (Figures 11d and 11e). The data shown here is for an entire run, complete with the initial ramping up of the course hence why there is a strong hysteresis effect. We compare an entire run, instead of only the falling limb as if sound is linked to white water, then that relationship should be true regardless of flow type and thus prove that white water is the source of sound. The hysteresis effect is lesser in the sound/WWV plot, meaning that even during rapid increases in discharge and unsteady flow, the white water still correlates with the sound.

When the sub-aerial sound and WWV are compared for different heights and configurations, we see a different pattern to that between sub-aerial sound and stage (Figure 7). Rather than an increase in RE height improving

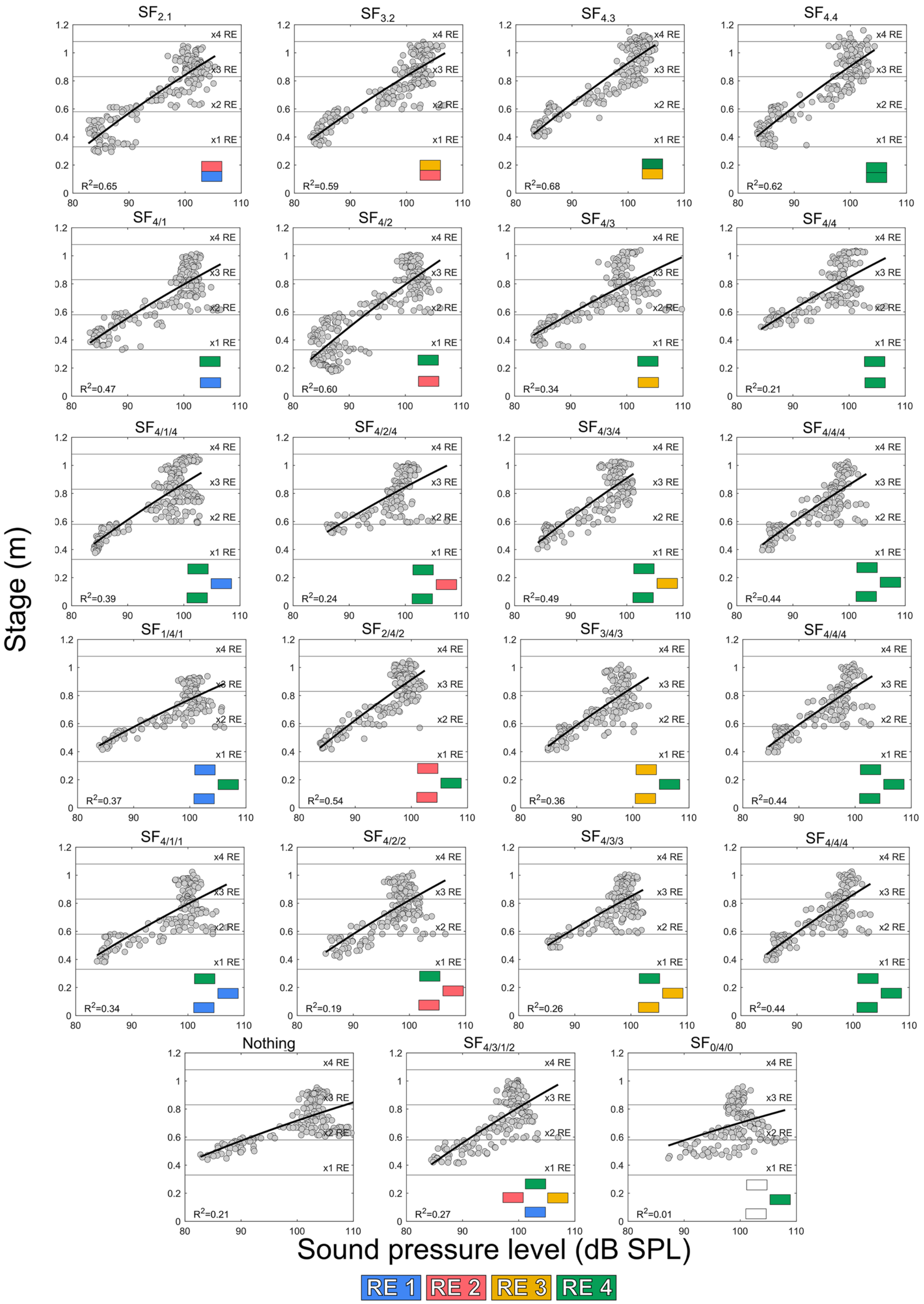

Figure 10. Plots showing the underwater sound pressure level and stage recorded during the mixed configuration experimental runs. Inset schematics have the block configuration color coded by the towers' height. Black line is the logarithmic function fitted to the data and the associated R^2 printed. Horizontal lines indicate the heights of the roughness element.

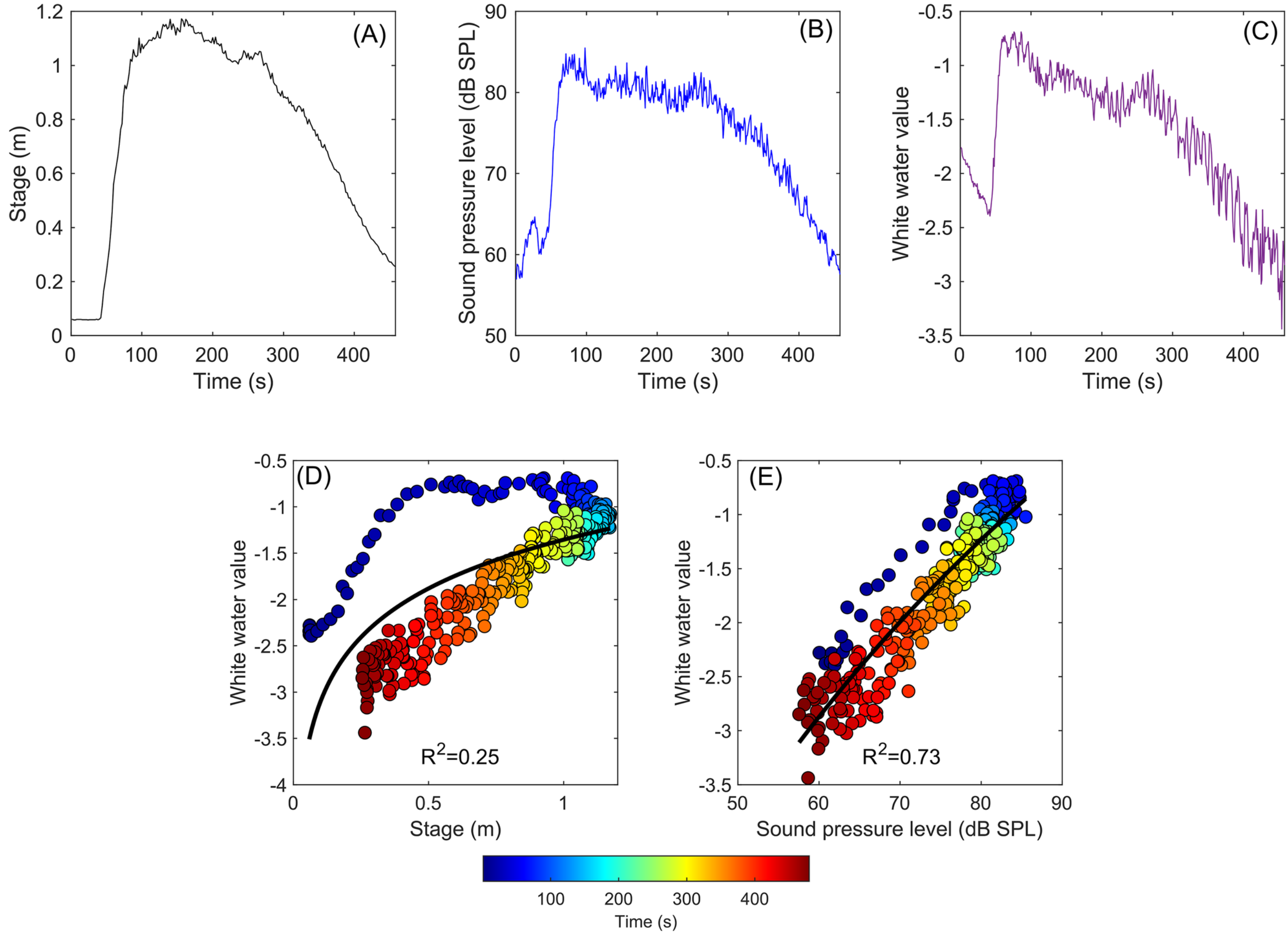

Figure 11. Data shown from experimental run $LF_{4.4}$. (a) Hydrograph, (b) sonohydrograph (sound), plotting sound-stage, (c) aphrosograph (foam), plotting sound-WWV, (d) relationship between stage and sound pressure level (SPL), and (e) relationship between white water value and SPL. Black line is a logarithmic function fitted to the data.

the relationship between sound and stage, Figure 12 has very similar R^2 of between 0.54 and 0.82 regardless of height. The only low R^2 value of 0.35 was with LF_1 in which there was a large range of WWV for a similar SPL. When there is low sound, <70 db SPL, there is a hockey stick shape to the data, primarily in LF_2 and $LF_{2.2}$. At these lower SPLs, as they increased, there was no substantial change in WWV, meaning at the early and closing stages of release, even as sound was being produced, there was little change in the WW being made. The data from LF_2, $LF_{2.2}$, and $LF_{3.3}$ has two distinct clusters of data, between low and high SPL, with gaps of WWV between them.

4. Discussion

4.1. RE Impact on Sub-aerial Sound

Our previous work linking sound to river stage indicated that the RE size was a determining factor on the relationship between sound and stage (Osborne et al., 2021). Here we tested the hypothesis that the height of the RE was the main controlling factor on sound. By comparing the R^2 values from the different RE configurations (Figure 13a), we see that as the height increases, so does the R^2, which provides support for our previous work. The height of the RE, rather than the configuration of the blocks, appears to cause the R^2 of the relationship between sound and stage. We find that a RE does not become inactive in sound generation once fully submerged, and still has an influence on flow at higher stages, as seen by the sound data not rapidly quietening after RE submergence (Figure 7). As the stage rises, it will first encounter the base of the block, and the flow is blind to

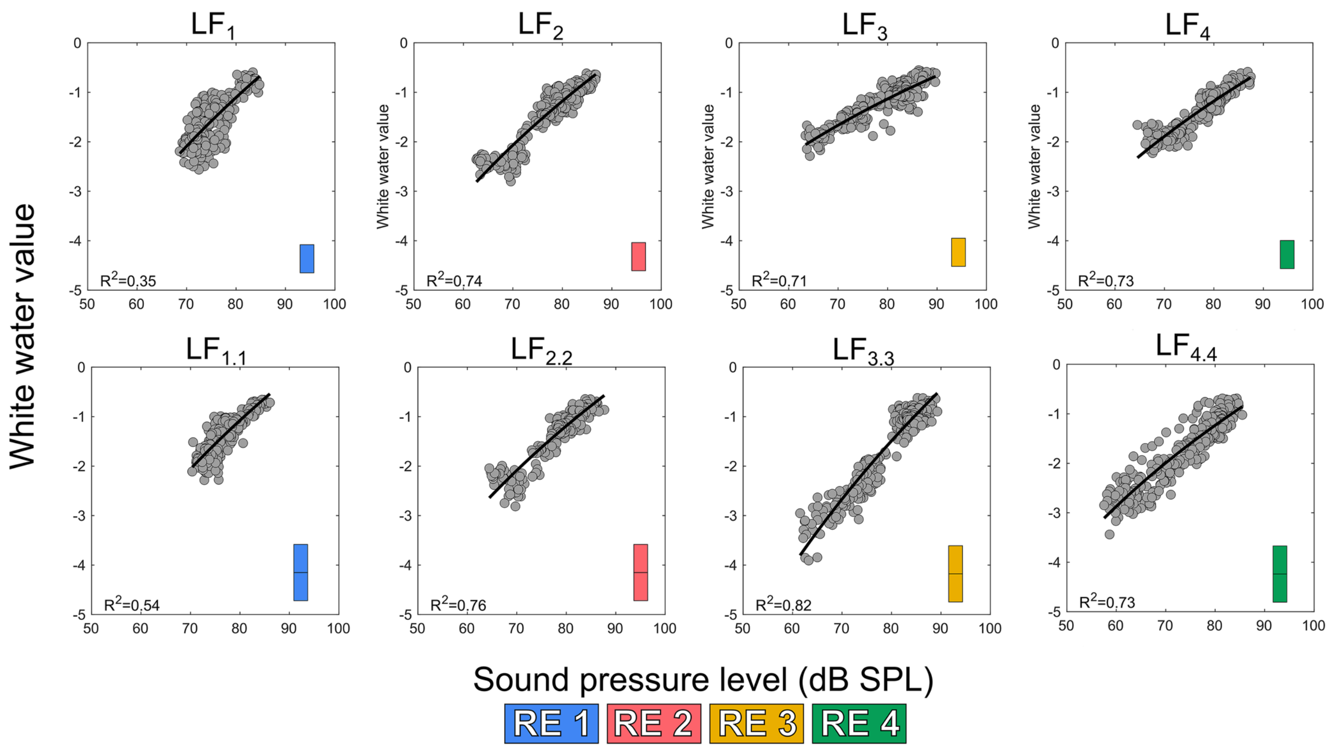

Figure 12. Plots showing the relationship between sub-aerial sound and white water value. Inset schematics show the block configuration color coded by the towers' height.

the height of the RE, so we expect to see that below the submergence of a block, any sound-stage relationship will be the same. Our data (Figures 7 and 8) suggest we see this blindness, with nearly identical data paths from the taller REs (Figure 14). We see kinks in the data when the flow reaches the point where it encounters the top of

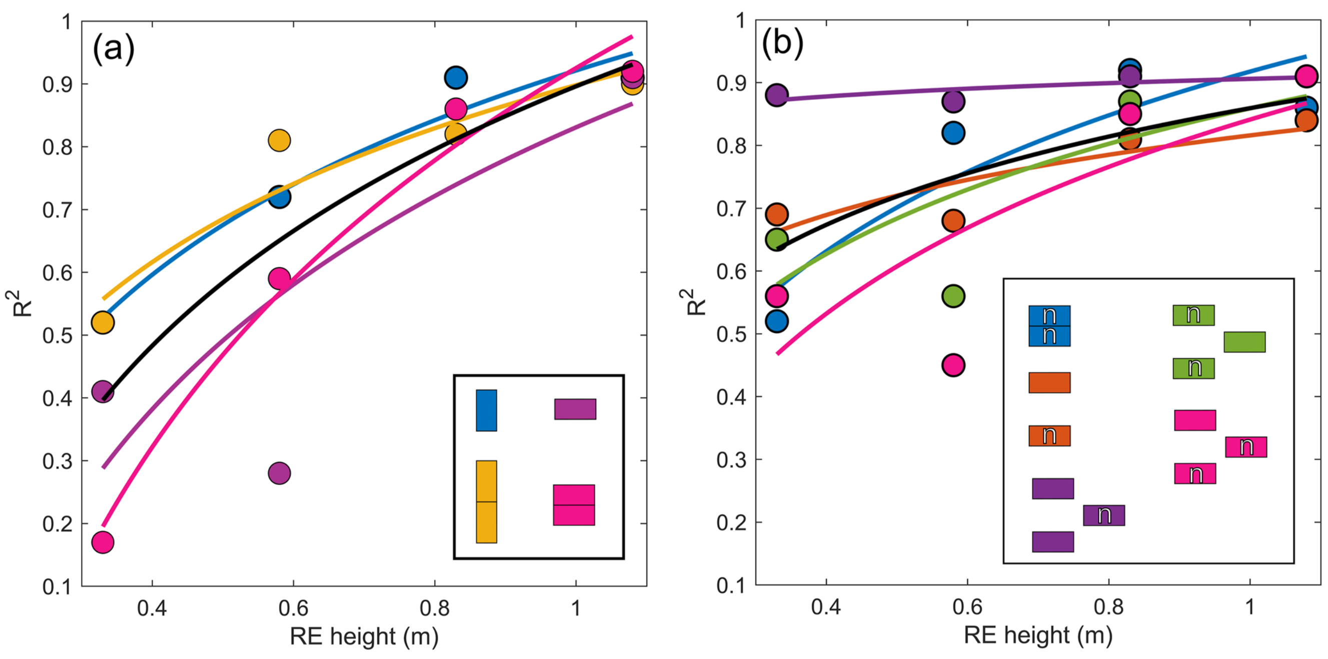

Figure 13. Synthesis figure of the R^2 values collected from each sub-aerial experimental run, broken into the (a) simple and (b) complex configurations. Complex configuration uses the block height that changed in each run. Black line indicates the average relationship found with increasing RE height.

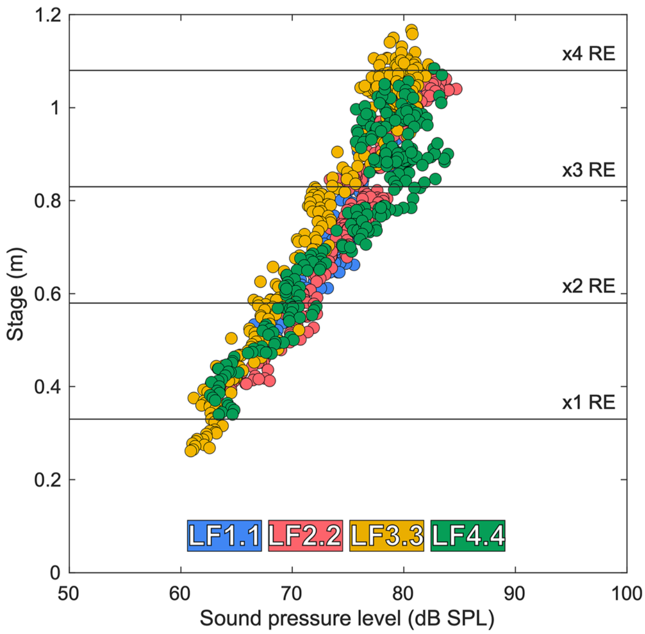

Figure 14. SPL plotted against stage for all $LF_{n1\cdot n1}$ block combinations.

the RE, for example, runs LF_1, $LF_{1.1}$, SF_1, and $SF_{1.1}$ in Figure 7, and causes a rapid loudening of the flow. The sudden change in SPL is linked to the height of the RE, with it occurring just after the flow overtops the block.

The free-surface is the dynamic and turbulent surface of the rivers' flow, and therefore is affected by flow disturbing REs (Muraro et al., 2021). Flammer et al. (1970) observed that as relative submergence increased, the flow transitions between three phases of pronounced, gradual and negligible free-surface effects. These free-surface effects are shown to be white water generating structures such as surface waves and riffles (Brocchini & Peregrine, 2001). Lawrence (2000) found at the point of partial submergence that there was high flow resistance and that as the RE continued to be submerged the resistance gradually reduced. Therefore, as an RE is overtopped, we do not see a cessation to the free-surface effects, but continue to observe them. At our maximum stage, an RE with height of 1 has a relative submergence of 2.85, whereas a RE with a height of 4 has a relative submergence of 0.87. This means that at the max stage, the RE1 and RE4 are respectively in the regions of gradual and pronounced free surface effects. At maximum stage, the RE of height 1 is still producing free surface effects, which would only become negligible at a stage of around 1.5 m. The larger RE 4 would require a stage of nearly 4 m to reduce any free-surface effects, therefore allowing sound to be measured beyond submergence. It is by the mechanism of REs becoming submerged, but still having free-surface effects, that we suggest why sound is produced, albeit at a reduced but stable rate, after the submergence of the RE.

The boundary layer is the region where a fluid flows over a solid body, such as our water over the blocks, in which velocity is zero at the boundary, and increases away from the boundary in a logarithmic velocity profile (Carling, 1992). After the submergence of a RE, factors such as RE arrangement and channel geometry were required for modeling the boundary. The kinked changes in SPL at the point when an RE is submerged (Figure 7) is from the mechanism of how the flow changes, as before submergence it could only go around the sides, forming a horseshoe vortex, and as stage increases, it can now overtop, creating a trailing vortex (Dey et al., 2008; Ouro et al., 2017). The change of vortex has an associated change in energy, with a horseshoe vortex releasing more energy than a trailing vortex (Zeman, 1995). The shape of the obstacle will influence the free-surface, generating drag, with Nardone and Koll (2016) finding that sharp angular obstacles (such as our block) produce the maximum amount of drag due to increasing flow separation. However, hemispherical object still produced drag and followed the same pattern of drag lessening as the RE became submerged further (Nardone & Koll, 2016). Simpson (1989) found that as flow separation occurs, turbulent flow forms, and thus white water is produced, so the larger or more angular the RE, the more flow separation that will happen. That results in more white water, which was shown to be linked to sound. Relative submergence and sound can be linked, with the stronger relationships between stage and sound occurring when REs have a lower relative submergence at maximum stage.

When considering a natural river channel, we do not expect to see a single block in the channel, or for every boulder to be the exact same size or shape. So by looking at more complex channel designs, by including different heights of blocks and configurations, we can go someway to create a more naturalistic setup. With a single RE, we find that RE height is the critical determinant of the sound-stage relationship, and so when there is a mixture of heights, we expect that the tallest RE will still be the most important. It is clear from the comparison in Figure 13 that the R^2 values are higher when there are multiple REs in the channel. Counterintuitively, creating less of an obstacle, makes the sound-stage relationship better. For example, the addition of a split level block configuration with $SF_{n1.n2}$, increases the R^2 with removing one block from $SF_{2.2}$ to make $SF_{2.1}$, increases R^2 from 0.59 to 0.86. We expect the presence of multiple heights act to smooth the abrupt transition from flow going around, to overtopping a RE, which created the sudden increases in SPL shown in SF_1 and $_{1.1}$. If that is played out in a natural environment, then a heterogeneous mix of RE heights would have influence on the sound being produced, helping to increase the correlation between sound and stage.

We cannot disregard the influence of shorter REs in a configuration, as although a mixture of heights may help smooth out the data, large varied heights may introduce scatter in the sound-stage relationship, for example, 10 and 100 cm REs. With $SF_{4/1}$ and $SF_{4/2}$, there is a block of four in each, however compared to other situations with a 4 block high tower, the R^2 is lower. At lower depths, the flow is again blind to the fact of smaller REs, with RE4 perhaps being a constant background sound, with the shorter RE acting independently as in SF_1. Without the smooth transition between two block heights, the sudden increases in SPL are back. In runs with an uneven distribution of block heights, the ability of taller blocks to dominate over the shorter ones becomes clear. For example, when two out of the three towers are four blocks high, the R^2 only varies between 0.87 and 0.91. Conversely, when only one of the towers is four blocks high, the shorter towers influence the sound-stage relationship greatly, with an R^2 range between 0.45 and 0.91. In an uneven distribution, the REs with the greatest number of similar heights may impose more of an impact than the spatial configuration of them. However, as the average height of the block increases, so does the R^2, meaning the taller the obstacles are, the better the relationship.

4.2. Sub-aerial Sound Generation

Knowing what is creating the sound we are trying to relate to stage will aid in the design of any future sub-aerial and river sound experiments. From the image analysis of how white water changes over stage, we are able to determine that white water correlates with SPL and infer that it is the white water producing the sound. Figure 11 demonstrates that on both rising and lower limbs, white water and sound maintain a logarithmic fit, unlike the relationship between white water and stage when there is a split between the limbs. In Figure 12, there is an R^2 of between 0.35 and 0.82, the fit between white water and stage is not perfect, with scatter still across the data. The scatter of the data could be a result of the camera position being oblique to the flow, introducing error in the WWV, or that the sound also introduces scatter since there can be a range of SPL for a single stage. There may be variation in the white water calculations due to small changes of luminance in an image, meaning greater or fewer pixels are categorized as white or black. Given that we did not have a light meter to measure that, we cannot be certain if imperceivable changes to light may have occurred. We presumed there are two zones of river sound production, from underwater and on the surface of the water. As our experiment lacked any mobile bedload, then it cannot account for the scatter of the data. In real-world examples in which there is mobile bedload, there may be an opportunity for sound to transmit from the water into the air, but it is dependent on the water depth, the frequency, and amplitude of the collision (Geay et al., 2019).

Some of the scatter between white water and sound may be due to the episodic nature of bubble formation and destruction. The exact moment between an image being taken and a recording being matched up could be out by milliseconds, for example, with bubble formations bursting within tens of milliseconds, the data could be out of sync (Chicharro & Vazquez, 2014). Averaging sound over an entire second should help to reduce the impact of that, whereas for the WWV, there is no averaging since only a frame was recorded per second. The recording of coastal breaking waves by Deane (1997) found air entrapment to generate sound underwater, with both the sound and breaking waves (creating white water when the air rises to the surface) occurring simultaneously. Peak sound production happened at the moment the wave broke, with it reducing as the wake decayed. A coastal wave is at a different physical and temporal scale to the waves generated in the WWC. Waves are being constantly being constructed and destructed in the WWC, and interacting with themselves, so rather than an episodic splosh of a wave, it combines into a melodic form. With potentially multiple sound sources from different REs, of differing intensity, duration, and frequency, taking a single video frame for reference may induce a minimal error but should not be completely out of sync.

4.3. Underwater Sound Generation From REs

With no bedload, the hydrophone used in our experiment would have two possible sources of sound, with Tonolla et al. (2009) finding during underwater flume experiments, noise was transmitted by white water at the surface, or from the pressure field formed around the hydrophone. We do not think that it is useful to construct relationships between stage and underwater sound because our data showed only a weak relationship between the two. Furthermore, in natural channels, they would be affected by the noise of bedload transport. Bedload transport has been shown to be active in the same frequency range that we observe sub-aerial sound at, at between 500 and 2,000 Hz and dependent on bedload size (Geay et al., 2017). Our data suggest that there is a direct correlation between underwater sound and stage up to a stage of 0.6 m, which may not be a good choice if concerned about flood monitoring, for example, but could influence other forms of monitoring, such as bedload since the frequencies overlap. Tonolla et al. (2009) identified that relative submergence of REs may cause changes in the underwater soundscape, particularly in lower-order streams. With that change in soundscape, we therefore may be seeing evidence as to why stage and underwater sound relationships are lesser than sub-aerial sound. Marineau et al. (2015) recorded the sound level of a flood event using a hydrophone, and attributed discharge in direct relation to the bed transport generated sound. Given that our data have underwater sound reacting in a similar manner without bedload, it could mean that the influence of the sound produced by the flow needs to be considered in future works.

4.4. Controls on WWV and Sound

Having identified where sound is being produced from, we now need to understand what in turn controls the white water production. Our experiment leads us to two conclusions regarding how the height of an RE and the spacing of them affects sound production. From our white water imaging (Figure 12), we see that as an RE gets taller, the R^2 of the sound-WWV fit increases from 0.35 at LF_1 to between 0.71 and 0.74 at the other heights. The WWV is similar to the same SPL on these graphs, at −2 WWV having an SPL range of 65–71 dB. The nature of the scatter can be partially explained by the height of the REs, with the shorter RE (LF_1) being submerged almost immediately, but in doing so producing white water and sound, hence why it has a narrow range of SPL. At taller REs (LF_3 and $_4$), there is sound produced, but with less white water since water is forced around for longer, instead of over the top. The larger range of SPL is what allows a better fit to be found.

When comparing a height change, but with a larger block face there is a similar pattern, with the R^2 of the fit increasing from 0.54 at $LF_{1.1}$ to between 0.73 and 0.82 at the other heights. How the downstream length of the obstacle affects the white water is seen by comparing LF_3 and LF_4 and $LF_{3.3}$ and $LF_{4.4}$, with the amount of white water being less in the side-by-side REs. We suggest that even though $LF_{4.4}$ provides a larger blockage to the flow compared to LF_4, it causes the flow to diverge more, which seems to reduce the amount of turbulence produced. The separation of data point clusters in $LF_{2.2}$ and $LF_{3.3}$ may be explained by the sudden generation of white water once these obstacles are overtopped, since there would be a significant rise in white water generation potential. From a white water and sound perspective, we can determine that as RE height increases, the larger the SPL range becomes and that the configuration of the blocks mimics but could add a new delay to sound being produced.

4.5. Lessons for Field Deployment of Sound Monitors

A sound monitor can be used in areas where traditional monitoring techniques for stage measurements are not feasible, such as a lack of infrastructure. The need to understand what it is within a river that generates a strong sound-stage relationship is therefore vital if sound monitoring is to be of use in fields such as flood monitoring. From our WWC experiment, we identify the following lessons that should improve a sound-stage relationship.

To draw comparisons between an entirely unnatural channel to a natural one has its drawbacks, such as that there is no active bedload, and that it condenses a hydroevent from hours into minutes. What we can take away is the interaction of flow and REs. The height of REs is important in the sound-stage relationship, with the higher the RE, the higher the R^2. This does not mean that you need a 1-m tall RE in a stream that only reaches 0.5 m, for example, as it all becomes relative to the flow itself. Our configurations with RE of 2 (0.58 m) high still can produce very good relationships in relation to stages of up to 1.2 m. So in a natural setting, an RE equivalent or up to 50% less than the anticipated maximum stage will offer a strong chance of a relationship, with the proviso still that the taller the RE, the better the relationship can be. It will be highly unlikely that a natural channel will have simply one RE within it, meaning that channels are more likely to have a heterogeneous mixture of REs. In that situation, having a distribution of REs will help to generate a smoother and more constrained sound-stage relationship.

The use of using image analysis to calculate the amount of white water on a river is a proof of concept, rather than a fully functional process. We advise that if the method was to be used in a comparative study that certain conditions would have to be kept. Aerial photography will provide the best view of the river, so therefore the use of a drone would be best, if the sound produced by it was minimal. Despite the oblique view of our images, we were still able to find relationships, but obscuring by the blocks was possible. The field of view (FOV) of the river surface also needs to be considered, as you need to observe the full extent of the white water generated from an obstacle. Having a narrow FOV would cutoff sections of the tail of a wave, for example, having too large a field is less of a concern unless other white water structures begin to appear that are not related to the RE being studied. We therefore recommend that the FOV is directly related to the size of the RE so as to observe its white water production without cropping out areas and not to introduce other structures into it. To compare between rivers would require that the total area being monitored is similar to allow comparison. The ability to calculate the amount of white water in a river temporally could also be useful for other disciplines such as gas exchange or identifying areas of flow resistance.

5. Conclusion

Our paper aimed to determine the source of sub-aerial sound and how the REs within a channel can affect the sound-stage relationship. Through the use of a large-scale experiment, we were able to closely mimic a real river and generate sounds of a similar type. Sub-aerial sound is concluded to be predominantly produced by white water generated by the interaction of flow with the RE. Identifying the mechanism for the creation of the sound enabled us to begin to test what other factors could influence sound-stage relationship. The height of the REs within a channel is the primary control on the strength of the sound-stage relationships. In terms of relative submergence, the lower the stage that is required to be monitored up until, the better the relationship will be. A heterogeneous mixture of REs does not degrade the relationship, and instead improves it. An uneven distribution, however, will begin to influence the relationship, with more tall REs stabilizing it, and more shorter REs destabilizing.

Although the experiment was run at real-world scale, it is not a complete analog of a real river's behavior. Sediment is not fixed to the bed like our blocks, but is mobile, meaning the configuration can change during a flood event. However, since spatial configuration is not a significant factor in the sound-stage relationship, and the sound from individual REs becomes melodic. If the balance of RE heights were to change, then that may begin to change the relationship. With continued research into sound mechanics of rivers in relation to REs, such as our experiment but in a fully natural setting, the size and spatial distribution could be represented by a singular component, such as the maximum RE height in the channel. All of which could be an aid in the possibility of being able to predict the sound so that you can use it as a proxy for stage.

Data Availability Statement

The data that support the findings of this study are available from DOI:10.17632/gxf5sy24kg.1.

Acknowledgments
This work was supported by Durham University, the British Society of Geomorphology, the European Regional Development Fund – Intensive Industrial Innovation Program Grant no. 25R17P01847, and Evolto Ltd. The authors also acknowledge the help of the team at the Tees Barrage International White Water Centre for all their help and assistance. We thank the anonymous reviewers for their invaluable comments and suggestions on the manuscript.

References

Barton, J. S., Slingerland, R. L., Gabrielson, T. B., & Johnson, P. A. (2005). Listening to bedload: A flume study relating acoustic response to bedload motion. *Proceedings of the Federal interagency sediment monitoring instrument and analysis workshop* (pp. 9–11).

Bathurst, J. C. (1978). Flow resistance of large-scale roughness. *Journal of the Hydraulics Division*, *104*(12), 1587–1603. https://doi.org/10.1061/jyceaj.0005114

Bolghasi, A., Ghadimi, P., & Feizi Chekab, M. A. (2017). Sound attenuation in air–water media with rough bubbly interface at low frequencies considering bubble resonance dispersion. *Journal of the Brazilian Society of Mechanical Sciences and Engineering*, *39*(12), 4859–4871. https://doi.org/10.1007/s40430-017-0852-3

Brocchini, M., & Peregrine, D. (2001). The dynamics of strong turbulence at free surfaces. Part 1. Description. *Journal of Fluid Mechanics*, *449*, 225–254. https://doi.org/10.1017/s0022112001006012

Carling, P. (1992). The nature of the fluid boundary layer and the selection of parameters for benthic ecology. *Freshwater Biology*, *28*(2), 273–284. https://doi.org/10.1111/j.1365-2427.1992.tb00584.x

Chan, W. H. R., Johnson, P. L., & Moin, P. (2021). The turbulent bubble break-up cascade. Part 1. Theoretical developments. *Journal of Fluid Mechanics*, *912*, A42. https://doi.org/10.1017/jfm.2020.1083

Chanson, H. (2012). (Chapter 7) Advective diffusion of air bubbles in turbulent water flows. In *Fluid mechanics of environmental Interfaces*. CRC Press.

Chanson, H., & Toombes, L. (1998). Supercritical flow at an abrupt drop: Flow patterns and aeration. *Canadian Journal of Civil Engineering*, *25*(5), 956–966. https://doi.org/10.1139/l98-013

Chicharro, R., & Vazquez, A. (2014). The acoustic signature of gas bubbles generated in a liquid cross-flow. *Experimental Thermal and Fluid Science*, *55*, 221–227. https://doi.org/10.1016/j.expthermflusci.2014.03.011

Deane, G. B. (1997). Sound generation and air entrainment by breaking waves in the surf zone. *Journal of the Acoustical Society of America*, *102*(5), 2671–2689. https://doi.org/10.1121/1.420321

Dey, S., Raikar, R. V., & Roy, A. (2008). Scour at submerged cylindrical obstacles under steady flow. *Journal of Hydraulic Engineering*, *134*(1), 105–109. https://doi.org/10.1061/(asce)0733-9429(2008)134:1(105)

Ferguson, R. (2010). Time to abandon the Manning equation? *Earth Surface Processes and Landforms*, *35*(15), 1873–1876. https://doi.org/10.1002/esp.2091

Flammer, G. H., Tullis, J. P., & Mason, E. S. (1970). Free surface, velocity gradient flow past hemisphere. *Journal of the Hydraulics Division*, *96*(7), 1485–1502. https://doi.org/10.1061/jyceaj.0002563

Geay, T., Belleudy, P., Gervaise, C., Habersack, H., Aigner, J., Kreisler, A., et al. (2017). Passive acoustic monitoring of bed load discharge in a large gravel bed river. *Journal of Geophysical Research: Earth Surface*, *122*(2), 528–545.

Geay, T., Michel, L., Zanker, S., & Robert Rigby, J. (2019). Acoustic wave propagation in rivers: An experimental study. *Earth Surface Dynamics*, *7*(2), 537–548. https://doi.org/10.5194/esurf-7-537-2019

Gomi, T., Sidle, R. C., & Richardson, J. S. (2002). Understanding processes and downstream linkages of headwater systems. *BioScience*, *52*(10), 905–916. https://doi.org/10.1641/0006-3568%282002%29052%5B0905:upadlo%5D2.0.co;2

Hall, R. O., Kennedy, T. A., & Rosi-Marshall, E. J. (2012). Air-water oxygen exchange in a large whitewater river. *Limnology and Oceanography: Fluids and Environments*, *2*(1), 1–11. https://doi.org/10.1215/21573689-1572535

Herbich, J. B., & Shulits, S. (1964). Large-scale roughness in open-channel flow. *Journal of the Hydraulics Division*, *90*(6), 203–230. https://doi.org/10.1061/jyceaj.0001133

Kean, J. W., & Smith, J. D. (2006). Form drag in rivers due to small-scale natural topographic features: 1. Regular sequences. *Journal of Geophysical Research*, *111*(F4), F04009. https://doi.org/10.1029/2006jf000467

Kolmogorov, A. (1949). On the fragmentation of drops in a turbulent flow. *Proceedings of the USSR Academy of Sciences*.

Lawrence, D. S. (2000). Hydraulic resistance in overland flow during partial and marginal surface inundation: Experimental observations and modeling. *Water Resources Research*, *36*(8), 2381–2393. https://doi.org/10.1029/2000wr900095

Leighton, T. (1994). The sound field. In *The acoustic bubble* (pp. 1–66). Elsevier. https://doi.org/10.1016/b978-0-12-441920-9.50006-7

Manasseh, R., Babanin, A. V., Forbes, C., Rickards, K., Bobevski, I., & Ooi, A. (2006). Passive acoustic determination of wave-breaking events and their severity across the spectrum. *Journal of Atmospheric and Oceanic Technology*, *23*(4), 599–618. https://doi.org/10.1175/jtech1853.1

Marineau, M. D., Minear, J. T., & Wright, S. A. (2015). Using hydrophones as a surrogate monitoring technique to detect temporal and spatial variability in bedload transport. *Paper presented at the 10th Federal interagency sedimentation conference* (p. 12).

Minnaert, M. (1933). XVI. On musical air-bubbles and the sounds of running water. *The London, Edinburgh, and Dublin Philosophical Magazine and Journal of Science*, *16*(104), 235–248. https://doi.org/10.1080/14786443309462277

Morse, N., Bowden, W. B., Hackman, A., Pruden, C., Steiner, E., & Berger, E. (2007). Using sound pressure to estimate reaeration in streams. *Journal of the North American Benthological Society*, *26*(1), 28–37. https://doi.org/10.1899/0887-3593(2007)26[28:uspter]2.0.co;2

Muraro, F., Dolcetti, G., Nichols, A., Tait, S. J., & Horoshenkov, K. V. (2021). Free-surface behaviour of shallow turbulent flows. *Journal of Hydraulic Research*, *59*(1), 1–20. https://doi.org/10.1080/00221686.2020.1870007

Nardone, P., & Koll, K. (2016). Drag force of elements mounted on a rough bed considering relative submergence (pp. 1–3).

Osborne, W. A., Hodge, R. A., Love, G. D., Hawkin, P., & Hawkin, R. E. (2021). Babbling brook to thunderous torrent: Using sound to monitor river stage. *Earth Surface Processes and Landforms*, *46*(13), 2656–2670. https://doi.org/10.1002/esp.5199

Ouro, P., Wilson, C. A. M. E., Evans, P., & Angeloudis, A. (2017). Large-eddy simulation of shallow turbulent wakes behind a conical island. *Physics of Fluids*, *29*(12), 126601. https://doi.org/10.1063/1.5004028

Powell, D. M. (2014). Flow resistance in gravel-bed rivers: Progress in research. *Earth-Science Reviews*, *136*, 301–338. https://doi.org/10.1016/j.earscirev.2014.06.001

Rodi, W. (2010). *Large eddy simulation of river flows* (pp. 23–32). River Flow.

Ronan, T. J., Lees, J. M., Mikesell, T. D., Anderson, J. F., & Johnson, J. B. (2017). Acoustic and seismic fields of hydraulic jumps at varying Froude numbers. *Geophysical Research Letters*, *44*(19), 9734–9741. https://doi.org/10.1002/2017gl074511

Schmandt, B., Gaeuman, D., Stewart, R., Hansen, S. M., Tsai, V. C., & Smith, J. (2017). Seismic array constraints on reach-scale bedload transport. *Geology*, *45*(4), 299–302. https://doi.org/10.1130/g38639.1

Simpson, R. (1989). Turbulent boundary-layer separation. *Annual Review of Fluid Mechanics*, *21*(1), 205–232. https://doi.org/10.1146/annurev.fl.21.010189.001225

Tonolla, D., Lorang, M. S., Heutschi, K., & Tockner, K. (2009). A flume experiment to examine underwater sound generation by flowing water. *Aquatic Sciences*, *71*(4), 449–462. https://doi.org/10.1007/s00027-009-0111-5

Ulseth, A. J., Hall, R. O., Boix Canadell, M., Madinger, H. L., Niayifar, A., & Battin, T. J. (2019). Distinct air–water gas exchange regimes in low- and high-energy streams. *Nature Geoscience*, *12*(4), 259–263. https://doi.org/10.1038/s41561-019-0324-8

Venditti, J. (2013). 9.10 – Bedforms in sand-bedded rivers. In *Treatise on geomorphology* (pp. 137–162). Elsevier. https://doi.org/10.1016/b978-0-12-374739-6.00235-9

Weichert, R., Minor, H., & Bezzola, G. (2006). Bed morphology and flow resistance in steep open channels with varying widths. In *River flow 2006*. Taylor & Francis. https://doi.org/10.1201/9781439833865.ch110

Zeman, O. (1995). The persistence of trailing vortices: A modeling study. *Physics of Fluids*, *7*(1), 135–143. https://doi.org/10.1063/1.868734